Optics & Laser Technology 170 (2024) 110255

Contents lists available at ScienceDirect

Optics and Laser Technology

journal homepage: www.elsevier.com/locate/optlastec

Full length article

Liquid crystal anisotropic axicon for the generation of non-diffracting Bessel beams with longitudinally varying polarization

Tomasz Jankowski [a], Noureddine Bennis [a], Anna Spadlo [a], José Francisco Algorri [b,c,d], María del Mar Sánchez-López [e,f,*], Ignacio Moreno [e,g]

[a] Faculty of Advanced Technologies and Chemistry, Military University of Technology, Warsaw 00-908, Poland
[b] Photonics Engineering Group, University of Cantabria, Santander, 39005, Spain
[c] CIBER de Bioingeniera, Biomateriales y Nanomedicina, Instituto de Salud Carlos III, 28029 Madrid, Spain
[d] Instituto de Investigación Sanitaria Valdecilla (IDIVAL), 39011 Santander, Spain
[e] Instituto de Bioingeniería. Universidad Miguel Hernández de Elche, E03202 Elche, Spain
[f] Departamento de Física Aplicada. Universidad Miguel Hernández de Elche, E03202 Elche, Spain
[g] Departamento de Ciencia de Materiales, Óptica y Tecnología Electrónica, Universidad Miguel Hernández de Elche, Avda. Universidad s/n, E03202 Elche, Spain

ARTICLE INFO

Keywords:
Axicon
Polarization
Bessel beams

ABSTRACT

In this work we demonstrate a tunable liquid–crystal element of linear phase profile along the radial coordinate. In combination with a regular refractive axicon, it behaves as an anisotropic axicon, generating the collinear superposition of two orthogonally polarized Bessel beams with different propagation constant. This superposition results in a Bessel beam where the state of polarization (SOP) varies periodically along propagation. Experimental results probe the voltage control of the SOP oscillating period, which agree well with theory. This compound axicon is a very compact and efficient way of generating Bessel beams with polarization modulation, thus representing a significant advantage over other methods reported in the literature that require bulk optical systems based on spatial light modulators.

1. Introduction

Since its introduction by Durnin [1,2], Bessel beams have been extensively studied because of their line focusing [3] and non-diffracting properties [4] that find applications in optical traps [5], biological imaging [6], materials' processing [7] or free-space optical communications [8]. Furthermore, their self-healing properties, i.e., their restoring capacity after an obstruction, have been exploited in classical and quantum systems [9,10]. The most efficient way to generate a Bessel beam is by means of a radially symmetric prism, also known as a conical lens or axicon [11]. Axicons can be fabricated either as refractive [12] or as diffractive components [13]. Refractive axicons are commercially available but their performance parameters (clear aperture and deflection angle) cannot be tuned by the user, since these parameters are set on fabrication. Instead, tunable diffractive axicons based on liquid–crystal technology make use of the optical phase modulation characteristic of liquid crystals. In this way, programmable axicons have been performed on liquid–crystal spatial light modulators (SLM) by encoding phase profiles that vary linearly along the radial coordinate [14,15]. Also, liquid–crystal arrays of tunable micro-axicon elements [16] and diffractive spiral axicons producing perfect vortex beams of tunable topological charge [17] have been demonstrated. All these systems generate Bessel beams of uniform polarization.

In general, Bessel beams present significant intensity variations along the depth of focus (DOF) distance. Typically, the on-axis intensity rises with propagation to a peak and then gradually declines towards the end of the DOF. In addition, imperfections in the axicon (for instance an oblate tip in a refractive axicon) can generate oscillations in the on-axis intensity distribution [18]. Therefore, several works have developed different techniques [18–21] to correct for these effects and engineer the axial intensity profile, typically to achieve a flat response, i.e. an optical needle, but also to achieve axial intensity ramps or arbitrary shapes.

Another interesting breakthrough was reported in [22] where Bessel beams with varying state of polarization (SOP) along propagation were demonstrated. This was achieved by performing a polarization sensitive axicon on an SLM. A double-pass though the SLM enabled to display two different diffractive axicons, each one affecting one of the two orthogonal linear polarization components and having a different period.

* Corresponding author at: Instituto de Bioingeniería. Universidad Miguel Hernández de Elche, E03202 Elche, Spain.
E-mail address: mar.sanchez@umh.es (M.M. Sánchez-López).

https://doi.org/10.1016/j.optlastec.2023.110255
Received 13 March 2023; Received in revised form 19 October 2023; Accepted 21 October 2023
Available online 28 October 2023

Consequently, the generated Bessel beam exhibited, along propagation, a varying phase-shift between these polarization components, thus resulting in a continuous variation of the SOP. The combination of such axicons with spiral phases led to higher-order vector Bessel beams with periodically varying polarization along propagation [23]. Such SOP oscillatory behavior was further demonstrated by producing two counter-propagating Bessel beams by means of a Sagnac interferometer [24], by an SLM-based common path interferometer [20] or by a polarization Fourier transform filtering system [25]. However, these are all bulk optical systems that require the use of SLMs together with beam splitters [22,23,25] or filtering in 4f systems [26], thus introducing important losses that significantly reduce the overall light efficiency.

Metasurfaces and nanogratings offer compact and very efficient ways to produce axicons, and they have been used to demonstrate wavelength independent Bessel beams [27] or higher-order vectorial Bessel beams [28]. These techniques are based on creating artificial birefringent optical elements by producing spatial microstructures. Therefore, they are useful to produce arbitrary polarization functions that vary along the optical path of the beam [29]. However, these optical elements are not tunable. Liquid-crystals (LC) exhibit natural birefringence and represent an alternative and well-stablished technology to build such devices and, most relevant, make them tunable through voltage control [30].

In this work we present a compact, efficient, and tunable polarization anisotropic axicon produced by combining a LC conical lens with a refractive axicon. While the refractive axicon equally deviates all polarization states, the LC element only adds or subtracts a conical phase to the polarization component parallel to the extraordinary index of refraction. Therefore, two orthogonally polarized Bessel beams with different inclination are generated, thus exhibiting a phase-shift along propagation. We use a refractive axicon of much higher power than the LC axicon; therefore, the Bessel beam length is basically determined by the refractive element, while the LC axicon controls the SOP modulation along propagation. The proposed tunable and compact anisotropic axicon could find applications in materials processing or optical traps, requiring the polarization modulation of the non-diffracting beam.

The work is organized as follows: after this introduction, Section 2 summarizes the basic concepts on axicons and Bessel beams that will be employed. Next, Section 3 describes the fabrication of the LC axicon and provides results for retrieving its radial phase retardance. The combination of the LC axicon with the refractive axicon is analyzed within the Jones matrix formalism since fully coherent and fully polarized light is considered. Section 4 discusses the experimental results where a Bessel beam with voltage-controlled polarization modulation along propagation is demonstrated. Results in the Fourier plane are included to illustrate the polarization splitting that confirms the superposition of the two collinear orthogonally polarized Bessel beams. Finally, the conclusions of the work are presented.

2. Axicons and bessel beams

A Bessel beam is a superposition of conical plane waves travelling at the same angle. It is a solution of the Helmholtz equation $\left[\nabla^2+k^2\right]g(x,y,z)=0$ which, expressed in cylindrical coordinates is written as

$$\nabla^2 g=\frac{\partial^2 g}{\partial r^2}+\frac{1}{r}\frac{\partial g}{\partial r}+\frac{1}{r^2}\frac{\partial^2 g}{\partial \theta^2}+\frac{\partial^2 g}{\partial z^2}=-k^2 g, \tag{1}$$

where $r=\sqrt{x^2+y^2}$ is the transversal radial coordinate and z the axial coordinate along the propagation direction, and has a solution $g(r,z)$ that takes an amplitude in the form of

$$g(r,z)=e^{ik_z z}J_0(k_r r). \tag{2}$$

Here J_0 is the zero-order Bessel function of first kind and $k=2\pi/\lambda$ is the modulus of the wavevector $\mathbf{k}=(k_x,k_y,k_z)$. $k_r=\sqrt{k_x^2+k_y^2}$ is the radial wavenumber and k_z is the axial wavenumber.

The Bessel beam transversal intensity distribution is proportional to $J_0^2(k_r r)$ and remains invariant (non-diffracting) along propagation, even in the presence of obstacles. Although ideal Bessel beams are not physically realizable, truncated Bessel beams that retain their properties along a certain distance can be indeed generated. Although initially demonstrated [2] by performing the Fourier transform of an annular transmission mask, the simplest method to generate a Bessel beam is by means of an axicon, a conical lens that directly generates the radial conical wavefront. Fig. 1(a) illustrates the phase of a diffractive axicon, where the period p of the radial blazed phase grating is related to the deflection angle by the diffraction grating law $\lambda/p=\sin(\theta)$. Hence, the radial wavenumber depends on the gratings period as $k_r=2\pi/p$. Fig. 1 (b) illustrates the generation of a Bessel beam behind the axicon and its propagation (Fig. 1(b)), and its transversal plane (Fig. 1(c)) and the parameters describing it. If we consider the plane where the axicon is located as the origin $z=0$, the maximum distance z_{max} where the Bessel beam extends is given by

$$z_{max}=r_{max}\frac{k_z}{k_r}=\frac{r_{max}}{\tan(\theta)}, \tag{3}$$

where r_{max} denotes the maximum radial extension of the axicon. θ is the deflection angle, i.e., the angular direction of $\mathbf{k}$ relative to the z axis, i.e., $\tan(\theta)=k_r/k_z$. The effective width W of the Bessel beam is determined by the first zero of the Bessel function J_0, which occurs at radius $r_0=2.4028/k_r$, thus

$$W=2r_0=\frac{0.766\lambda}{\sin(\theta)}. \tag{4}$$

In the usual paraxial approximation regime, the small angle approximation can be applied in Eqs. (3) and (4).

3. Materials and methods

3.1. Liquid-crystal axicon

In this work we use the transmission-electrode technique to produce a tunable LC axicon with controllable radial wavenumber. This technique has been previously applied in other LC axicons [31–33] operating under linearly polarized light and producing a Bessel beam with uniform polarization. Other types of LC tunable optical elements such as Powell lenses [34] and aspherical lenses [35–37] have been demonstrated with the same technique. The structure is simple, can be fabricated in one lithographic step, and only requires two voltage sources. It consists of an ITO electrode that produces a high resistance through a high aspect ratio design. Therefore, the current is low, but the voltage is continuous along the electrode. Then, this voltage is homogeneously distributed by a set of floating concentric electrodes across the active area, similarly to a modal lens [38] but avoiding the requirement of high-resistivity layers. The structure used in this work is like that of [36]. After the patterning process to achieve the transmission electrode on ITO coated glass, a polyimide alignment layer is spin-coated on the patterned substrates. This layer is rubbed to obtain a molecular homogeneous alignment. Following the rubbing treatment, the LC axicon device was assembled by dispensing a photopolymerizable epoxy (NOA68) seal on the perimeter of one substrate, while high precision 80 μm silica sphere spacers were dispersed on the opposing substrate. The two substrates were placed with antiparallel alignment, namely with opposite rubbing directions. Finally, a LC mixture having positive dielectric anisotropy and high birefringence [39] was infiltrated into the cavity.

Fig. 2 shows the results obtained with this LC device. Fig. 2(a) illustrates the optical setup. A He-Ne laser, spatially filtered and collimated with lens L1, illuminates the LC axicon. A first linear polarizer (P1) polarizes the light beam along the 45° direction with respect to the LC director axis (indicated vertical with the blue dot in the figure).

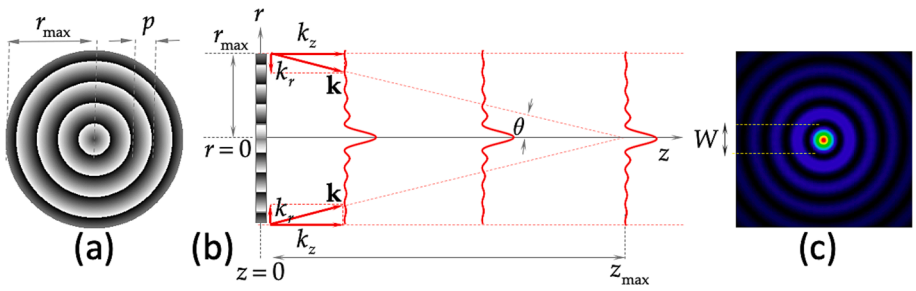

Fig. 1. Illustration of the (a) Axicon phase. (b) Bessel beam propagation. (c) Intensity of a transversal plane.

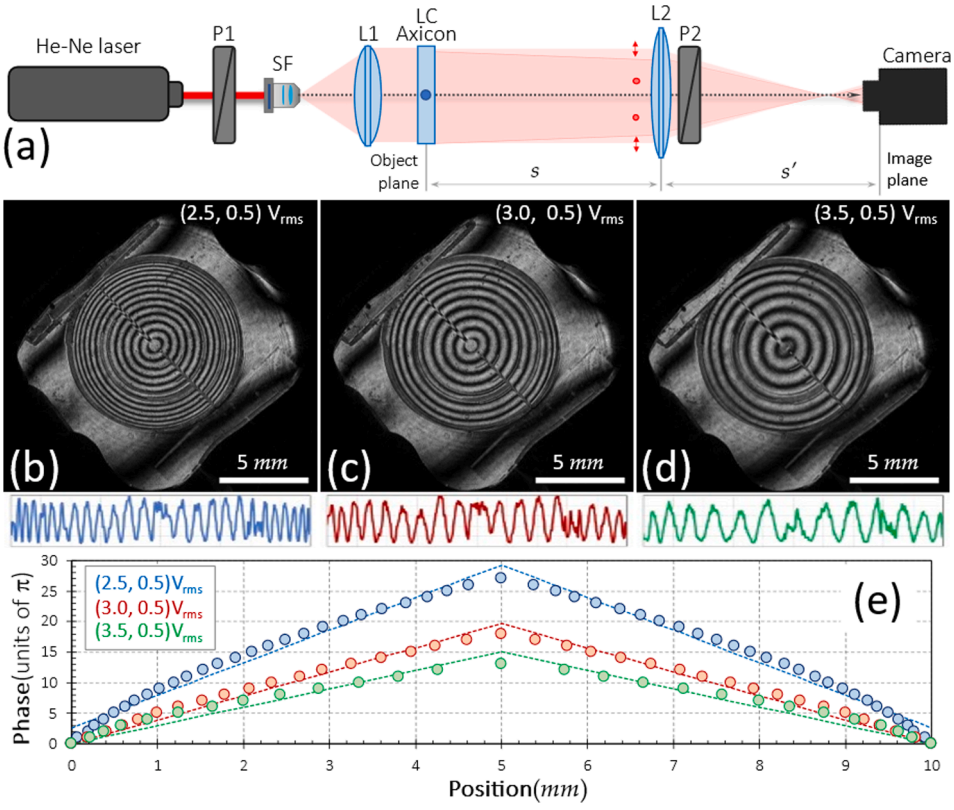

Fig. 2. (a) Scheme of the optical setup for imaging the LC axicon: LP: linear polarizers, SF: spatial filter, L: converging lenses. (b)-(d) Captures of the interference pattern for different applied voltages (below each image the insets show the intensity profile along a diameter in the central active area). (e) Retrieved phase profile along the horizontal direction and its best linear fit.

Therefore, the vertical polarization component is affected by the LC device and the radial linear phase deviates this component towards the beam axis. On the contrary, the horizontal linear polarization component is unaffected and remains collimated. Thus, except for a constant phase term, the Jones matrix describing this LC axicon can be written as

$$\mathbf{M}_{LC}(r) = \begin{bmatrix} 1 & 0 \\ 0 & \exp[i\phi(r)] \end{bmatrix}, \tag{5}$$

where $\phi(r)$ is the radially dependent retardance which, ideally, should be linear with r as $\phi(r) = k_r^{LC} r$ being k_r^{LC} the radial wavenumber imparted by the LC axicon device.

By now placing a second polarizer (P2) also oriented at 45° behind the LC axicon, the two polarization components interfere and the Jones vector after the polarizer reads as

$$\mathbf{J}_{out}(r) = \frac{1}{\sqrt{2}} \begin{bmatrix} 1 & 1 \\ 1 & 1 \end{bmatrix} \bullet \mathbf{M}_{LC}(r) \bullet \mathbf{J}_{in} = \frac{1}{2}\{1 + \exp[\phi(r)]\} \begin{bmatrix} 1 \\ 1 \end{bmatrix}, \tag{6}$$

where $\mathbf{J}_{in} = \frac{1}{\sqrt{2}}[1 \quad 1]^T$ (T indicating the transpose vector) is the normalized Jones vector standing for the input beam, and $\mathbf{P}_{45} = \frac{1}{\sqrt{2}} \begin{bmatrix} 1 & 1 \\ 1 & 1 \end{bmatrix}$ is the Jones matrix of the second polarizer. The output field intensity is given by $I(r) = \mathbf{J}_{out}^{\dagger} \bullet \mathbf{J}_{out} = \cos^2[\phi(r)/2]$, where † indicates the Hermitian complex-conjugate vector.

We visualize this interference to verify the LC axicon retardance. For that purpose, a second converging lens (L2) with focal length f' is used to image the LC axicon plane on a camera detector plane, simply by adjusting the lens distances to the axicon (s) and the camera (s') to fulfill the imaging condition $1/s + 1/s' = 1/f'$. Fig. 2(b), 2(c) and 2(d) show three examples of the interference pattern $I(r)$ captured by the camera when different V_{rms} voltages are applied to the device. Specifically, the same fixed voltage (0.5 V_{rms}) is set at the axicon center (through the electrode without the concentric electrodes attached), whereas a different higher voltage (2.5, 3.0 and 3.5 V_{rms}) is applied at the axicon perimeter (through the concentric electrodes) to obtain a different

positive (i.e. convergent) axicon in each example. The voltages are selected so that the variable transmission line voltage distribution compensates for the non-linearity of the birefringence curve. Well-contrasted interference rings are visible within a circular active area of radius $r_{max} = 5mm$, indicating that the LC retardance ϕ varies along the radial coordinate. In the central active region, a narrow diagonal line with inverted interference corresponding to the electrode transmission line is observed. In the outer region, where there is no modulation, some interference lines are also visible in Fig. 2(b-d), indicating certain nonuniformity in the LC layer. Nevertheless, the central active region where the optical modulation is produced, shows radial interference patterns that change with voltage, denoting a behaviour close to that expected for the LC axicon.

As mentioned, for a LC axicon ϕ must vary linearly with the radial coordinate as $\phi(r) = k_r^{LC} r$. Below each image in Fig. 2(b-d), the inset shows the intensity profile along a diameter in the central circular active area of the LC aperture. The separation between fringes appears approximately constant (as opposed to the more common case where the phase is made proportional to r^2 to produce a lens [36]). Note that as the V_{rms} applied at the device perimeter increases, the number of interference rings decreases. This means a lower slope of the linear phase along r, a larger period value p of the axicon phase function and, consequently, a smaller deflection angle. In each case, the retardance $\phi(r)$ is retrieved from the interference patterns $I(r) = \cos^2[\phi(r)/2]$. Fig. 2(e) shows the measured phase profile $\phi(r)$ along the central horizontal line retrieved from these interferograms. Despite some slightly parabolic shape at the center and at the edges, $\phi(r)$ approximates rather well a linear radial phase variation in all three cases. The best linear fit is also included in the graph, with correlation values above $R^2 > 0.98$ in the three cases. Hence, the resulting phase profile is almost linear when proper voltages are applied.

These results prove the effective realization of a tunable LC axicon, where the angle of the deflected beam can be controlled with the applied V_{rms} voltage. However, only the polarization parallel to the LC director is deflected, and the maximum phase variation is only about $k_r^{LC} r_{max} \simeq 27\pi$ along the aperture. Therefore, the deflection angle is very small and the production of the Bessel beam is not efficient. Angles of only 0.097, 0.071 and 0.053 degrees are retrieved from the slopes of the linear fit to the phase profiles in Fig. 2(e).

3.2. Compound liquid-crystal and refractive axicon

To achieve higher deflection powers and obtain an anisotropic compound axicon, we combine the previous LC axicon with a refractive glass axicon. The refractive axicon is a commercial component (Thorlabs, model AX252-A) made of UV fused silica, with a clear aperture of $25mm$ and a deflection angle of 0.9 degrees (one order of magnitude greater than those obtained with the LC axicon). The combination of the LC axicon, affecting only the vertical polarization component, and the refractive axicon, equally affecting the horizontal and vertical polarization components, results in a new Jones matrix $\mathbf{M}_C(r)$ for the compound axicon given by

$$\mathbf{M}_C(r) = \exp\left(ik_r^R r\right)\mathbf{M}_{LC}(r) = \begin{bmatrix} \exp(ik_{r\perp} r) & 0 \\ 0 & \exp(ik_{r\parallel} r) \end{bmatrix}, \tag{7}$$

where k_r^R denotes the radial wavenumber imparted by the refractive axicon, and where we assumed a perfect LC axicon with $\phi(r) = k_r^{LC} r$. Eq. (7) shows that the compound axicon behaves as a linear anisotropic axicon with wavenumbers $k_{r\perp} = k_r^R$ and $k_{r\parallel} = k_r^R + k_r^{LC}$ for polarization components crossed and parallel to the LC director axis (in this case they coincide with the horizontal and vertical polarization components respectively). The latter (i.e. $k_{r\parallel}$) can be tuned thanks to the properties of the LC axicon.

4. Experimental results

4.1. Bessel beam with polarization change along propagation

The effective performance of the compound axicon is the superposition of two Bessel beams: 1) one Bessel beam with horizontal polarization, generated only by the refractive axicon, and 2) a slightly shorter Bessel beam with vertical polarization, generated by the combined effect of the LC axicon and the refractive axicon. The phase retardation between these two orthogonally polarized Bessel beams increases linearly with propagation distance (z). As a result, the SOP changes as the Bessel beam propagates. Namely, the transversal radial retardance between the vertical and horizontal polarization components at the compound axicon plane is $(k_{r\parallel} - k_{r\perp})r = k_r^{LC} r$, which provokes a retardance $(k_{z\parallel} - k_{z\perp})z$ in the Bessel beam along the axial direction. This effect was already achieved in [21] by displaying two axicon functions into a LC-SLM in an optical arrangement designed to modulate both polarization components. However, it required a bulk optical system with very low efficiency. Here instead, an equivalent effect is simply achieved by means of the compound axicon in a much effective and compact system.

Fig. 3(a) illustrates the optical setup to probe the generated Bessel beam. The compound axicon was illuminated with linearly polarized light oriented at $+45^\circ$ to have equal weights in the horizontal and vertical components. The Bessel beam arises shortly after the compound axicon. We moved the camera detector along the axis to capture the beam at different axial distances measured from the axicon. For each position, the SOP variation along the axis was verified using polarizer P2. A quarter-wave plate (QWP) was added before P2 when measuring the right (R) and left (L) circular components. Fig. 3(b) shows the experimental results of the Bessel beam generated behind the compound axicon at four different axial distances and for applied voltages (3.0, 0.5) V_{rms} (case in Fig. 2(c)). At each distance, the beam was analyzed with the six typical polarization analyzers (linear analyzers oriented horizontally, vertically, diagonal at $\pm 45^\circ$, and R and L circular analyzers).

Images in Fig. 3 were deliberately saturated to clearly visualize the Bessel beam pattern. In all cases, the bright spot surrounded by concentric rings, characteristic of the Bessel beam, is confirmed. Note that the SOP of the central spot is changing with the distance. For each distance, the yellow arrow indicates the analyzer that cancels the central spot, thus showing that the Bessel beam has the orthogonal polarization. For instance, at $z = 76mm$ the beam is linearly polarized at $+45^\circ$, since the central bright spot cancels when the linear analyzer is oriented at -45°. On the contrary, the polarization of the Bessel beam becomes R circular, linear at -45° and L circular for distances $z = 84mm$, $z = 92mm$ and $z = 100mm$, respectively. Therefore, these results confirm the expected behavior: the superposition of two equally intense colinear Bessel beams with horizontal and vertical polarizations and phase shift difference that increases linearly upon propagation.

The axial retardance varies as $(k_{z\parallel} - k_{z\perp})z$, hence producing a periodic variation of the polarization state when it changes by 2π. According to the deflection angles derived from the results in Fig. 2, periods p of $23mm$, $31mm$ and $42mm$ are expected for the applied voltages (2.5, 0.5), (3.0, 0.5) and (3.5, 0.5) V_{rms} respectively. Fig. 4 shows the intensity of the Bessel beam center as a function of the propagation distance between 75 and $200mm$. Here the Bessel beam is observed between polarizer P1 oriented at 45° and a circular polarizer consisting of a QWP and polarizer P2.

The FLIR BFS-U3-28S5M-C camera was placed on the STANDA 8MT195X-840–10 motorized stage. The stage speed was set to 40 steps per second with a step of 0.025 mm and a camera frame rate of 10 fps. These settings allowed capturing 8-bit gray level images of the optical field shifted by 0.1 mm along the optical axis frame to frame. The camera exposure time and gain were set and fixed so that the images would not be overexposed in any camera position, i.e., the maximum

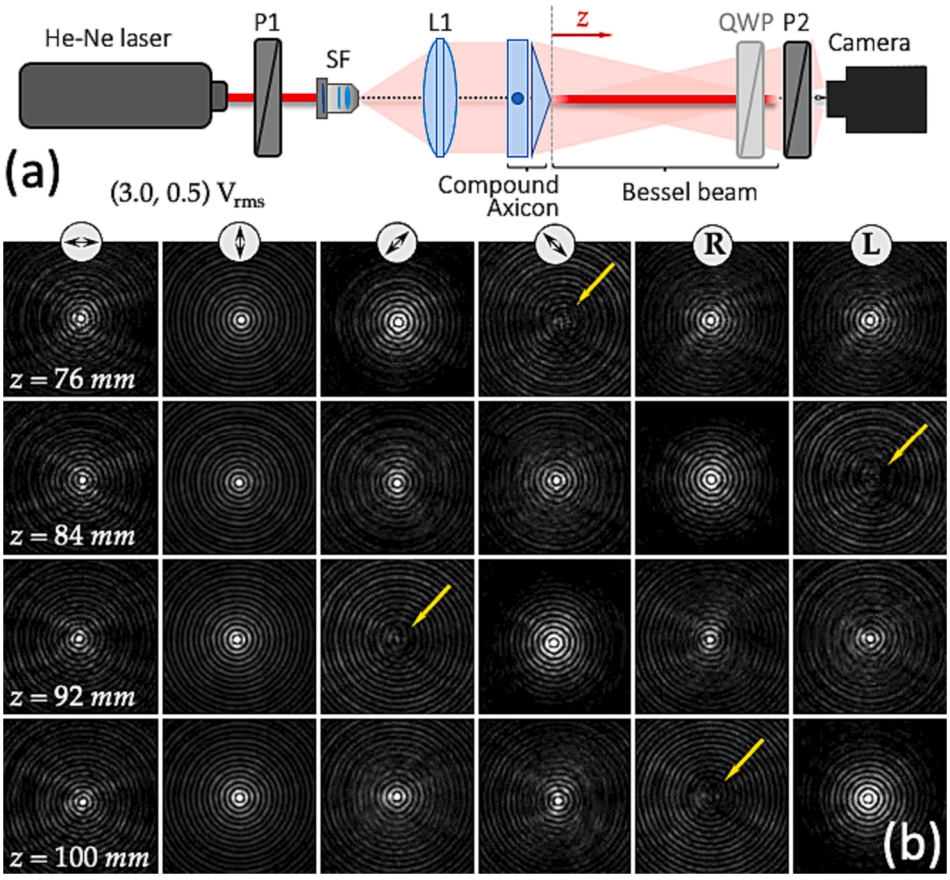

Fig. 3. (a) Optical system for analyzing the Bessel beam generated with the compound axicon, where z denotes the axial distance from the compound axicon. (b) Experimental captures at four axial distances for six different polarization analyzers and applied voltages (3.0, 0.5) V_{rms}. Yellow arrows indicate the situations where the center of the Bessel beam is extinguished. (For interpretation of the references to colour in this figure legend, the reader is referred to the web version of this article.)

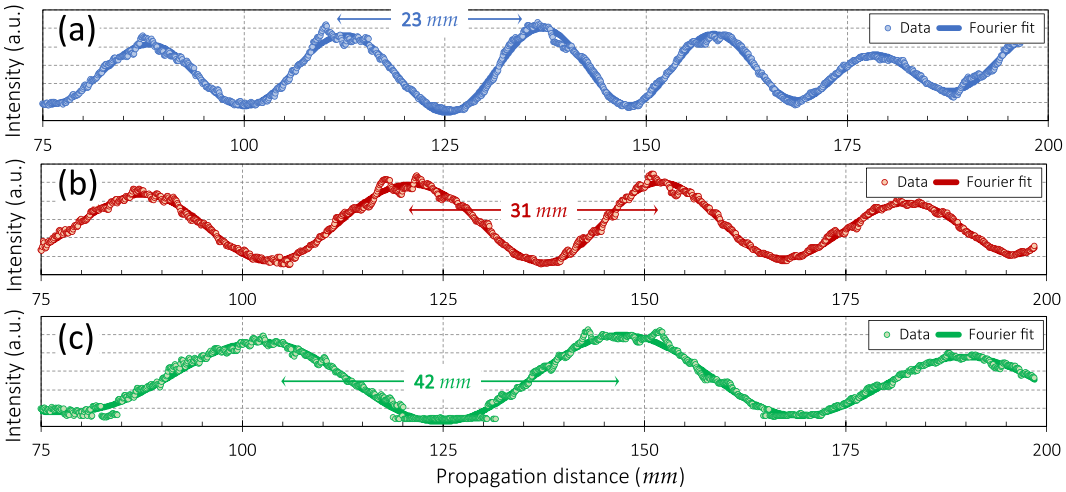

Fig. 4. Intensity along the propagation distance with the LC axicon tuned with (a) (2.5, 0.5) V_{rms}, (b) (3.0, 0.5) V_{rms} and (c) (3.5, 0.5) V_{rms}. The arrows indicate the expected periods for the three cases.

pixel value in the captured images did not exceed level 254. To measure the intensity of the central spot of the Bessel beam, the images were cropped and the average intensity at 10 neighboring pixels of maximal intensity was calculated. The discrete data function of intensity variation with propagation distance was later fitted to the Fourier series function by MATLAB Curve Fitter tool. Acquired curves were normalized to the maximal intensity. Fig. 4 show the results. Although they are affected by experimental errors arising from the LC device, the curves confirm the expected oscillatory behaviour. The oscillation is faster with z for the axicon with applied voltage (2.5, 0.5) V_{rms} and it becomes slower for higher voltages since the LC axicon phase decreases. The arrows in Fig. 4 indicate the expected spatial periods for the three cases, which match quite well the experiments.

Fig. 5 shows the normalized Stokes parameters in the case with (3.0,

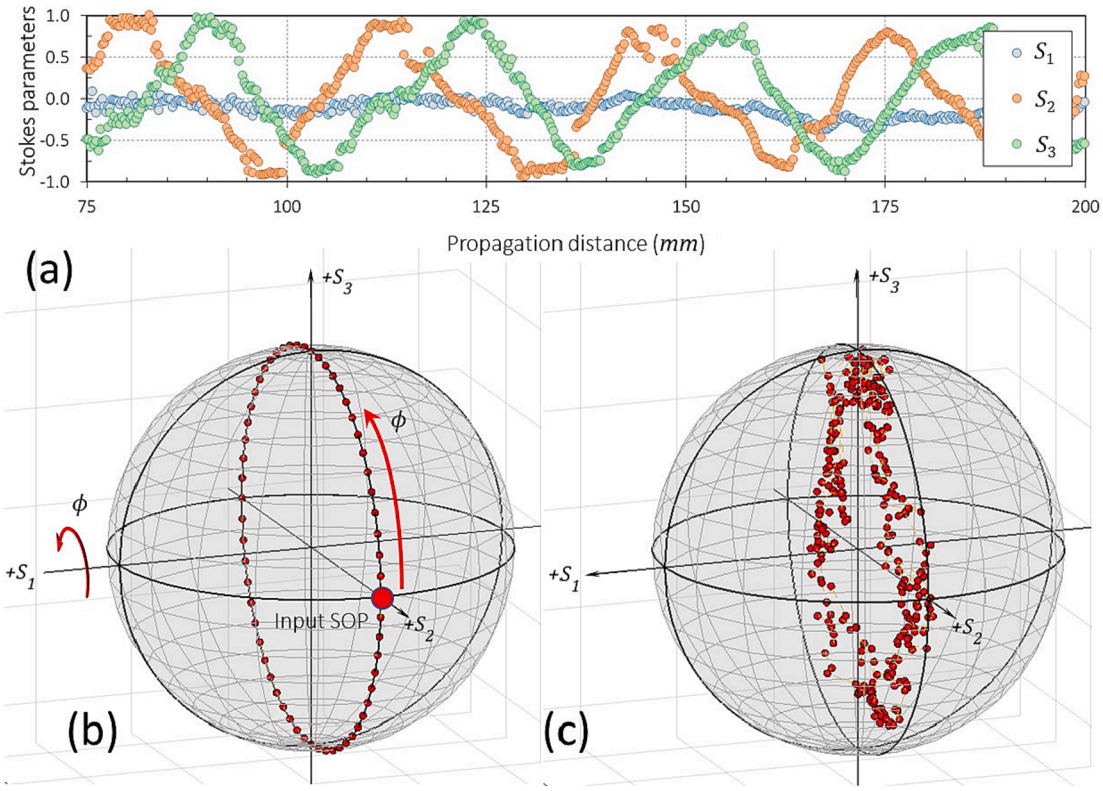

Fig. 5. (a) Experimentally measured normalized Stokes parameters as a function of the propagation distance for case (3.0, 0.5) V_{rms}. (b) Ideal theoretical SOP trajectory in the Poincaré sphere along propagation. (c) Experimental SOP trajectory derived from the data in (a).

0.5) V_{rms}. For this voltage, measurements were repeated using different polarization analyzers in front of the camera: a linear polarizer analyzer oriented horizontally, vertically, diagonal (45°) and antidiagonal (135°), and a right and a left circular polarizer. Thus, six axial curves were measured: $I_H(z)$, $I_V(z)$, $I_D(z)$, $I_A(z)$, $I_R(z)$ and $I_L(z)$, from which the normalized Stokes parameters shown in Fig. 5(a) are calculated for each axial distance z as:

$$S_1(z) = \frac{I_H(z) - I_V(z)}{I_H(z) + I_V(z)}, \tag{8a}$$

$$S_2(z) = \frac{I_D(z) - I_A(z)}{I_D(z) + I_A(z)}, \tag{8b}$$

$$S_3(z) = \frac{I_R(z) - I_L(z)}{I_R(z) + I_L(z)}. \tag{8c}$$

The curves in Fig. 5(a) show the axial SOP variation: the Stokes parameter S_1 remains approximately at $S_1 = 0$ along the path, while the Stokes parameters S_2 and S_3 show a periodic variation with z, with an axial displacement of a quarter period.

Fig. 5(b) represents the expected SOP variation visualized in the Poincaré sphere (PS). Since the input light is linearly polarized at 45°, its location on the PS is on the positive S_2 axis (indicated as input SOP in Fig. 5(b)). The compound axicon creates a linear retardance $\phi(z)$ between the horizontal and vertical polarization components. It is known [40] that the effect of a retarder can be obtained by rotating the PS an angle ϕ around the axis defined by the retarder's fast and slow axes, in this case the S_1 axis. Therefore, ideally, the SOP variation of the Bessel beam should yield a trajectory in the PS along the meridian in the S_2–S_3 plane (plane $S_1 = 0$), as depicted in Fig. 5(b). The circle is completed every period of oscillation. Fig. 5(c) shows that the trajectory retrieved from the experimental data in Fig. 5(a) with the experimental points all located approximately on the S_2 –S_3 plane, bears good agreement with theory.

4.2. Polarization splitting at the Fourier plane

A final verification of the LC compound axicon is presented in Fig. 6. Here, instead of regarding the Bessel beam generated in the near field, we look in the far field, where it is well-known that an axicon generates a narrow ring [41]. To do this, the optical system is now changed to a Fourier transform system by including a lens behind the axicon and now looking at its back focal plane (Fig. 6(a)). The compound axicon is located on the front focal plane of the lens to achieve an exact Fourier transform. The size of the Fourier transform ring is given by $f' \tan(\theta)$. In this case the lens focal length is $f' = 300mm$, thus, considering the angle $\theta = 0.9$ degrees of the refractive axicon, the ring of light on the camera detector should have a radius of $4.7mm$.

Fig. 6(b) shows the Fourier transform of the axicon when the input polarizer (P1) is perpendicular to the LC director axis. In this situation only the refractive axicon affects the input beam and a single narrow ring is observed. Fig. 6(c) shows a zoomed image of the square area in Fig. 6(b). The inset curve in Fig. 6(c) is the intensity profile along the diagonal direction indicated with the red line. Fig. 6(d) shows equivalent results when the input polarizer is oriented at 45°, thus having equal weights of horizontal and vertical polarization components incident on the LC axicon. In this situation, the ring in the Fourier transform is split in two, one ring for each polarization component. Since the LC axicon adds small additional power to the refractive axicon, the separation is very small. Nevertheless, the zoomed image in Fig. 6(e) clearly shows this double ring. The inner ring has the same location as the ring in Fig. 6 (b)-6(c) and it is polarized perpendicular to the LC director axis. This is the part of the beam not affected by the LC axicon. On the contrary, the outer ring is polarized parallel to the LC director axis and has a slightly greater radius, since this polarization is affected by both the LC axicon and the refractive axicon. These results agree with the formal analysis in section III B. Some weak additional rings arise due to the non-perfect linear phase profiles shown in Fig. 2(e), as clearly revealed by the

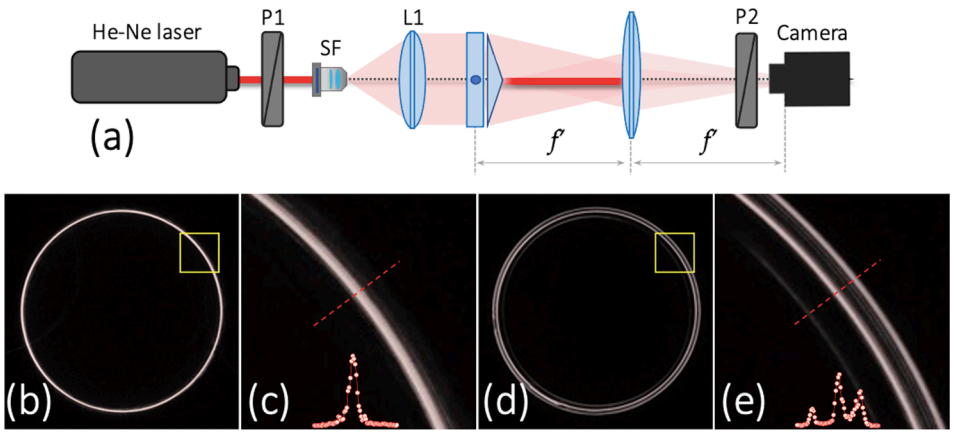

Fig. 6. (a) Optical system for analyzing the Fourier transform ring generated with the compound axicon. (b-c) Experimental ring for input linear polarization perpendicular to the LC director axis. (d-e) Experimental ring split for input linear polarization at 45° to the LC director axis. The inset curves in (c) and (e) show the intensity profile along the indicated diagonal line.

intensity profile shown in Fig. 6(e).

5. Conclusions

In summary, we have presented a new compound axicon device able to generate Bessel beams with polarization variation along the propagation distance. The device combines a regular refractive axicon with a LC tunable axicon. The latter only affects the polarization component of the input beam parallel to the LC director. Therefore, when the device is illuminated with linearly polarized light oriented at 45°, the compound axicon produces the collinear superposition of two Bessel beams with slightly different propagation constant. The result is a Bessel beam where the SOP changes periodically along the propagation distance. The LC axicon phase profile can be tuned by applying different V_{rms} values, therefore changing the spatial period of oscillation in the Bessel beam. The measured periods of the SOP variation are within centimeters and match quite well the expected results. Furthermore, the polarization splitting caused by the LC axicon has been observed in the Fourier transform domain. This compound axicon is a very compact and efficient way of generating Bessel beams with polarization modulation, thus representing a great advantage over other methods reported in the literature [22–26] that require bulk optical systems and SLMs.

The tunable LC axicon was fabricated using the transmission-electrode technique. The device operates as intended, although it shows slight deviations from the ideal linear radial retardance and certain non-uniformity. Despite these imperfections, the fabricated LC axicon device has proved useful in building the intended proof-of-concept of a compound axicon with tunable polarization modulation of the Bessel beam, where the spatial period of oscillation matches quite well the theoretical result.

CRediT authorship contribution statement

Tomasz Jankowski: Investigation, Methodology, Software, Writing – review & editing. **Noureddine Bennis:** Conceptualization, Investigation, Methodology, Supervision, Validation, Writing – review & editing. **Anna Spadlo:** Investigation, Methodology, Supervision, Writing – review & editing. **José Francisco Algorri:** Investigation, Methodology, Supervision, Validation, Writing – review & editing. **María del Mar Sánchez-López:** Conceptualization, Investigation, Methodology, Supervision, Validation, Writing – original draft. **Ignacio Moreno:** Conceptualization, Methodology, Supervision, Writing – review & editing.

Declaration of Competing Interest

The authors declare that they have no known competing financial interests or personal relationships that could have appeared to influence the work reported in this paper.

Data availability

Data will be made available on request.

Acknowledgements

NB and AS acknowledge financial support from Military University of Technology, Poland (ref.: UGB 22-791). TJ acknowledges financial support from Actphast4R innovation Project. JFA acknowledges financial support from PID2019-107270RB-C21 and TED2021-130378B-C21 projects funded by MCIN/AEI/10.13039/501100011033, FEDER, and EU NextGenerationEU/PRT. MMSL and IM acknowledge financial support from Ministerio de Ciencia e Innovación, Spain (ref.: PID2021-126509OB-C22) and Generalitat Valenciana (ref. CIAICO/2021/276).

References

[1] J. Durnin, Exact solutions for nondiffracting beams. I. The scalar theory, J. Opt. Soc. Am. A 4 (4) (1987) 651–654.
[2] J. Durnin, J.J. Miceli Jr., J.H. Eberly, Diffraction free beams, Phys. Rev. Lett. 58 (1987) 1499–1501.
[3] V. Jarutis, R. Paškauskas, A. Stabinis, Focusing of Laguerre-Gaussian beams by axicon, Opt. Commun. 184 (2000) 105–112.
[4] D. McGloin, K. Dholakia, Bessel beams: diffraction in a new light, Contemp. Phys. 46 (1) (2005) 15–28.
[5] J. Arlt, V. Garces-Chavez, W. Sibbett, K. Dholakia, Optical micromanipulation using a Bessel light beam, Opt. Commun. 197 (2001) 239–245.
[6] K.-S. Lee, J.P. Rolland, Bessel beam spectral-domain high-resolution optical coherence tomography with micro-optic axicon providing extended focusing range, Opt. Lett. 33 (15) (2008) 1696–1698.
[7] M. Duocastella, C.B. Arnold, Bessel and annular beams for materials processing, Laser Photon. Rev. 6 (5) (2012) 607–621.
[8] Z. Lu, Z. Guo, M. Fan, M. Guo, C. Li, Y. Yao, H. Zhang, W. Lin, H. Liu, B. Liu, Tunable Bessel beam shaping for robust atmospheric optical communication, J. Light. Technol. 40 (15) (2022) 5097–5106.
[9] M. McLaren, T. Mhlanga, M.J. Padgett, F.S. Roux, A. Forbes, Self-healing of quantum entanglement after an obstruction, Nat. Commun. 5 (2014) 3248.
[10] C. Vetter, R. Steinkopf, K. Bergner, M. Ornigotti, S. Nolte, H. Gross, A. Szameit, Realization of free-space long-distance self-healing Bessel beams, Laser & Photonics Rev. 13 (2019) 1900103.
[11] G. Scott, M. McArdle, Efficient generation of nearly diffraction-free beams using an axicon, Opt. Eng. 31 (1992) 2640–2643.
[12] X.-F. Lin, Q.-D. Chen, L.-G. Niu, T. Jiang, W.-Q. Wang, H.-B. Sun, Mask-free production of integratable monolithic micro logarithmic axicon lenses, J. Light. Technol. 28 (8) (2010) 1256–1260.
[13] S. Doshay, D. Sell, J. Yang, R. Yang, J.A. Fan, High-performance axicon lenses based on high-contrast, multilayer gratings, APL Photon. 3 (2018), 011302.

[14] J.A. Davis, J. Guertin, D.M. Cottrell, Diffraction-free beams generated with programmable spatial light modulators, Appl. Opt. 32 (31) (1993) 6368–6370.
[15] Z. Jaroszewicz, V. Climent, V. Durán, J. Lancis, A. Kolodziejczyk, A. Burvall, A. T. Friberg, Programmable axicon for variable inclination of the focal segment, J. Mod. Opt. 51 (2004) 2185–2190.
[16] J.F. Algorri, V. Urruchi, N. Bennis, J.M. Sánchez-Pena, Modal liquid crystal micro-axicon array, Opt. Lett. 39 (12) (2014) 3476–3479.
[17] J. Pereiro-García, M. García-de-Blas, M.A. Geday, X. Quintana, M. Caño-García, Flat variable liquid crystal diffractive spiral axicon enabling perfect vortex beams generation, Sci. Rep. 13 (2023) 2385.
[18] T. Čižmár, K. Dholakia, Tunable Bessel light modes: engineering the axial propagation, Opt. Express 17 (18) (2009) 15558–15570.
[19] R. Dharmavarapu, S. Bhattacharya, S. Juodkazis, Diffractive optics for axial intensity shaping of Bessel beams, J. Optics 20 (8) (2018), 085606.
[20] S. Orlov, A. Juršėnas, E. Nacius, Optical Bessel-like beams with engineered axial phase and intensity distribution, J. Laser Micro Nanoeng. 13 (3) (2018) 244–248.
[21] P. Gotovski, P. Šlevas, S. Orlov, O. Ulčinas, A. Urbas, Generation of an optical needle beam with a laser inscribed Pancharatnam-Berry phase element under imperfect conditions, Opt. Express 29 (21) (2021) 33331–33345.
[22] I. Moreno, J.A. Davis, M.M. Sánchez-López, K. Badham, D.M. Cottrell, Nondiffracting Bessel beams with polarization state that varies with propagation distance, Opt. Lett. 40 (23) (2015) 5451–5454.
[23] J.A. Davis, I. Moreno, K. Badham, M.M. Sánchez-López, D.M. Cottrell, Nondiffracting vector beams where the charge and the polarization state vary with propagation distance, Opt. Lett. 41 (10) (2016) 2270–2273.
[24] P. Li, Y. Zhang, S. Liu, L. Han, H. Cheng, F. Yu, J. Zhao, Quasi-Bessel beams with longitudinally varying polarization state generated by employing spectrum engineering, Opt. Lett. 41 (20) (2016) 4811–4814.
[25] P. Li, D. Wu, Y. Zhang, S. Liu, Y. Li, S. Qui, J. Zhao, Polarization oscillating beams constructed by copropagating optical frozen waves, Photonics Res. 6 (7) (2018) 756–760.
[26] W.-Y. Wang, J.-X. Guo, S. Liu, J.-Q. Lü, Z.-W. Lu, Manipulating the variation of polarization during propagation along arbitrary circular trajectory of the Poincaré sphere, Appl. Phys. Lett. 121 (2022), 161102.
[27] W.T. Chen, M. Khorasaninejad, A.Y. Zhu, J. Oh, R.C. Devlin, A. Zaidi, F. Capasso, Generation of wavelength-independent subwavelength Bessel beams using metasurfaces, Light: Sci. & Appl. 6 (5) (2017) e16259.
[28] J. Baltrukonis, O. Ulčinas, S. Orlov, V. Jukna, High-order vector Bessel-gauss beams for laser micromachining of transparent materials, Phys. Rev. Appl. 16 (3) (2021), 034001.
[29] A.H. Dorrah, N.A. Rubin, A. Zaidi, M. Tamagnone, F. Capasso, Metasurface optics for on-demand polarization transformations along the optical path, Nat. Photonics 15 (2021) 287–296.
[30] J. Beeckman, K. Neyts, P.J.M. Vanbrabant, Liquid-crystal photonic applications, Opt. Eng. 50 (8) (2011), 081202.
[31] J.F. Algorri, P. Morawiak, N. Bennis, D.C. Zografopoulos, V. Urruchi, L. Rodríguez-Cobo, L.R. Jaroszewicz, J.M. Sánchez-Pena, J.M. López-Higuera, Positive-negative tunable liquid crystal lenses based on a microstructured transmission line, Sci. Rep. 10 (2020) 10153.
[32] J.F. Algorri, P. Morawiak, D.C. Zografopoulos, N. Bennis, A. Spadlo, L. Rodríguez-Cobo, L.R. Jaroszewicz, J.M. Sánchez-Pena, J.M. López-Higuera, Multifunctional light beam control device by stimuli-responsive liquid crystal micro-grating structures, Sci. Rep. 10 (2020) 13806.
[33] J. Stevens, T. Galstian, Electrically tunable liquid crystal lens with a serpentine electrode design, Opt. Lett. 47 (2022) 910–912.
[34] J.F. Algorri, P. Morawiak, D.C. Zografopoulos, N. Bennis, A. Spadlo, L. Rodríguez-Cobo, L.R. Jaroszewicz, J.M. Sánchez-Pena, J.M. López-Higuera, Cylindrical and Powell liquid crystal lenses with positive-negative optical power, IEEE Photon. Technol. Lett. 32 (2020) 1057–1060.
[35] A. Pusenkova, O. Sova, T. Galstian, Electrically variable liquid crystal lens with spiral electrode, Opt. Commun. 508 (2022), 127783.
[36] N. Bennis, T. Jankowski, P. Morawiak, A. Spadlo, D.C. Zografopoulos, J. M. Sánchez-Pena, J.M. López-Higuera, J.F. Algorri, Aspherical liquid crystal lenses based on a variable transmission electrode, Opt. Express 30 (2022) 12237–12247.
[37] J.F. Algorri, D.C. Zografopoulos, L. Rodríguez-Cobo, J.M. Sánchez-Pena, J. M. López-Higuera, Engineering aspheric liquid crystal lenses by using the transmission electrode technique, Crystals 10 (2020) 835.
[38] A.F. Naumov, M.Y. Loktev, I.R. Guralnik, G.V. Vdovin, Liquid-crystal adaptive lenses with modal control, Opt. Lett. 23 (1998) 992–994.
[39] N. Bennis, T. Jankowski, O. Strzezysz, A. Pakuła, D.C. Zografopoulos, P. Perkowski, J.M. Sánchez-Pena, J.M. López-Higuera, J.F. Algorri, A high birefringence liquid crystal for lenses with large aperture, Sci. Rep. 12 (2022) 14603.
[40] M.M. Sánchez-López, P. García-Martínez, A. Martínez-García, I. Moreno, Poincaré sphere analysis of a ferroelectric liquid crystal optical modulator: application to optimize the contrast ratio, J. Opt. A Pure Appl. Opt. 11 (2009), 015507.
[41] K. Yang, H. Luo, P. Li, F. Wen, Y. Gu, Z. Wu, Controlling spacing of double-ring perfect optical vortex using the Fourier transform of Bessel beam with axicon phase, Opt. Laser Technol. 158 (2023), 108881.